Chinese Journal of Natural Medicines

Macrocyclic trichothecenes from *Myrothecium verrucaria* PA 57 and their cytotoxic activity

Jisong MO, Yufen TAN, Wenjing AI, Yunyun LI, Yiyun YUAN, Yueping JIANG, Kangping XU, Guishan TAN, Wenxuan WANG, Jing LI, Shao LIU

Citation: Jisong MO, Yufen TAN, Wenjing AI, Yunyun LI, Yiyun YUAN, Yueping JIANG, Kangping XU, Guishan TAN, Wenxuan WANG, Jing LI, Shao LIU, Macrocyclic trichothecenes from *Myrothecium verrucaria* PA 57 and their cytotoxic activity, Chinese Journal of Natural Medicines, 2024, 22(9), 854−863. doi: 10.1016/S1875−5364(24)60573−X.

View online: https://doi.org/10.1016/S1875−5364(24)60573−X

Available online at www.sciencedirect.com
ScienceDirect
Chinese Journal of Natural Medicines 2024, **22**(9): 854-863
doi: 10.1016/S1875-5364(24)60573-X
Chinese Journal of Natural Medicines

•Original article•

Macrocyclic trichothecenes from *Myrothecium verrucaria* PA 57 and their cytotoxic activity

MO Jisong[1, 2], TAN Yufen[1], AI Wenjing[2], LI Yunyun[2], YUAN Yiyun[2], JIANG Yueping[1], XU Kangping[2], TAN Guishan[1, 2], WANG Wenxuan[2], LI Jing[1, 2*], LIU Shao[1*]

[1] *Department of Pharmacy, National Clinical Research Center for Geriatric Disorders, Xiangya Hospital, Central South University, Changsha 410008, China;*
[2] *Xiangya School of Pharmaceutical Sciences, Central South University, Changsha 410008, China*

Available online 20 Sep., 2024

[ABSTRACT] Four novel macrocyclic trichothecenes, termed mytoxins D−G (**1**−**4**), along with four known analogs (**5**−**8**), were isolated from the ethyl acetate extract of fermented rice inoculated with the fungus *Myrothecium verrucaria* PA57. Each compound features a tricyclic 12,13-epoxytrichothec-9-ene (EPT) core. Notably, mytoxin G (**4**) represents the first instance of a macrocyclic trichothecene incorporating a glucosyl unit within the trichothecene structure. The structures of the newly identified compounds were elucidated through comprehensive spectroscopic analysis combined with quantum chemical calculations. All isolated compounds demonstrated cytotoxic activity against the CAL27 and HCT116 cell lines, which are models for human oral squamous cell carcinoma and colorectal cancer, respectively. Specifically, mytoxin D (**1**) and mytoxin F (**3**) exhibited pronounced cytotoxic effects against both cancer cell lines, with IC_{50} values ranging from 3 to 6 nmol·L^{-1}. Moreover, compounds **1** and **3** were found to induce apoptosis in HCT116 cells by activating caspase-3.

[KEY WORDS] Macrocyclic trichothecenes; *Myrothecium verrucaria*; Cytotoxicity; Secondary metabolite; Soil fungi
[CLC Number] R284, R965 **[Document code]** A **[Article ID]** 2095-6975(2024)09-0854-10

Introduction

Trichothecenes, which are sesquiterpenoid mycotoxins with a tricyclic 12,13-epoxytrichothec-9-ene (EPT) core [1], are produced by various fungi, including *Fusarium* [2], *Trichoderma* [3], *Trichothecium* [4], and *Myrothecium* [5, 6]. To date, about 200 structurally distinct trichothecenes have been identified [1], and these can be divided into two main groups: macrocyclic and simple trichothecenes [7]. Macrocyclic trichothecenes are distinguished by an additional ring formed through esterification of the hydroxy groups at C-4 and C-15 of the EPT core, while simple trichothecenes lack this macrolide ring. Moreover, macrocyclic trichothecenes can be further classified into roridins, which have a C_{29}-skeleton, and verrucarins, which have a C_{27}-skeleton [8]. Due to their unique and complex structures with multiple chiral centers, trichothecenes exhibit a broad spectrum of bioactivities, including antimicrobial [9-12], antimalarial [13-16], and cytotoxic effects [17-19]. Recent studies have focused on their anticancer properties, given their potent cytotoxicity [20-24]. For example, roridin E has shown significant cytotoxicity against breast cancer cell lines, with IC_{50} values as low as 0.05 nmol·L^{-1} [17]. Consequently, trichothecenes are considered promising lead compounds for anticancer drug development. Further exploration of trichothecenes with low toxicity and high specificity in their biological activities is essential for advancing drug research.

In our ongoing quest to discover structurally diverse and biologically valuable compounds from soil fungi [25, 26], we isolated a strain of *Myrothecium verrucaria* PA57 from a soil sample collected at Daweishan Forest Park (28.427 10 °N, 114.089 85 °E). Metabolic profiling of the fermentation extract from *M. verrucaria* PA57, conducted using LC/MS, confirmed the presence of trichothecenes. To obtain sufficient quantities of the metabolites, large-scale fermentations

[Received on] 12-Jan.-2024
[Research funding] This work was supported by the National Natural Science Foundation of China (No. 82173713), the Natural Science Foundation of Hunan Province (Nos. 2021JJ41000 and 2021JJ40812), the Key Research and Development Program of Hunan Province (No. 2022SK2031), the Project of Hunan Administration of Traditional Chinese Medicine (No. B2023059), and the Postgraduate Scientific Research Innovation Project of Hunan Province (No. CX20230323).
[*]**Corresponding author]** E-mails: lijingliyun@csu.edu.cn (LI Jing); liushao999@csu.edu.cn (LIU Shao)
These authors have no conflict of interest to declare.

were subsequently performed, leading to the identification of four previously undescribed macrocyclic trichothecenes (**1**−**4**) and four known congeners (**5**−**8**) (Fig. 1). The structures of the novel compounds were elucidated through comprehensive analysis of HR-ESI-MS and NMR data, supplemented by gauge-independent atomic orbital (GIAO) NMR and electronic circular dichroism (ECD) calculations. Additionally, we assessed the *in vitro* cytotoxicity of all isolates against human oral squamous cell carcinoma (CAL27) and human colorectal cancer (HCT116) cell lines using the CCK-8 assay, with 5-fluorouracil as the positive control. Herein, we report the isolation, structural characterization, and cytotoxic evaluation of these compounds.

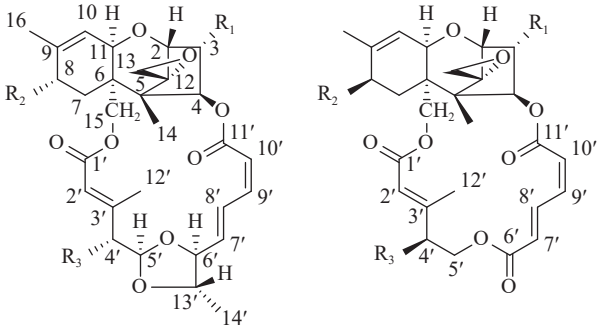

	R_1	R_2	R_3
1	OH	H	OH
2	H	OAc	OH
5	H	OAc	H
6	H	H	OH

	R_1	R_2	R_3
3	H	H	OH
4	OGlu	H	H
7	H	H	H
8	H	OH	H

Fig. 1 Structures of compounds 1−8.

Results and Discussion

Compound **1** was obtained as a white amorphous powder. Its molecular formula was determined to be $C_{29}H_{36}O_{10}$ based on HR-ESI-MS data, which showed a peak at *m/z* 562.2687 $[M + NH_4]^+$ (Calcd. for $C_{29}H_{40}NO_{10}$, 562.2647), indicating twelve degrees of unsaturation. The ^1H NMR spectrum (Table 1) revealed six olefinic protons at δ_H 7.59 (1H, t, *J* = 13.5 Hz, H-8'), 6.56 (1H, t, *J* = 11.3 Hz, H-9'), 5.93 (1H, br d, *J* = 15.3 Hz, H-7'), 5.83 (1H, d, *J* = 11.3 Hz, H-10'), 5.75 (1H, br s, H-2'), and 5.52 (1H, br s, H-10), eight oxygenated methines at δ_H 5.56 (1H, br s, H-4), 5.27 (1H, br d, *J* = 5.0 Hz, H-5'), 4.47 (1H, br d, *J* = 4.2 Hz, H-3), 4.09 (1H, m, H-6'), 4.01 (1H, br s, H-11), 3.84 (1H, brd, *J* = 5.0 Hz, H-4'), 3.65 (1H, H-2), and 3.65 (1H, H-13'), four methylenes including two oxygenated at δ_H 4.40 (1H, d, *J* = 12.6 Hz, H-15a), 4.06 (1H, d, *J* = 12.6 Hz, H-15b), 3.05 (1H, br s, H-13a), 2.78 (1H, br s, H-13b), 2.02 (2H, m, H-8), and 1.90 (2H, m, H-7), and four methyl groups at δ_H 0.82 (3H, s, H-14), 1.37 (3H, br s, H-14'), 1.73 (3H, s, H-16), and 2.26 (3H, s, H-12'). The ^{13}C NMR spectrum (Table 2) displayed 29 carbons, inclusive of two ester carbonyls (δ_C 166.3, 166.0), eight olefinic carbons (δ_C 155.8, 143.4, 140.4, 135.0, 126.0, 119.7, 118.9, 118.4), indicative of the presence of four double bonds, eight oxygenated sp^3 methines (δ_C 103.4, 82.5, 82.2, 79.7, 79.4, 76.6, 76.4, 68.8), three sp^3 quaternary carbons including one oxygenated (δ_C 64.7, 49.5, 44.0), four methylenes including two oxygenated (δ_C 63.4, 47.3, 27.7, 20.6), and four methyl groups (δ_C 23.5, 16.1, 13.4, 7.4). Detailed analysis of 1D and 2D NMR data confirmed that compound **1** is a macrocyclic trichothecene analog of roridin J [27].

A further examination of the ^1H–^1H correlation spectroscopy (COSY) and heteronuclear multiple bond correlations (HMBC) data for **1** (Fig. 2) revealed the presence of two distinct substructures: a trichothecene moiety and a macrocyclic lactone moiety. The trichothecene moiety was confirmed through ^1H–^1H COSY correlations (H-2/H-3/H-4, H-7/H-8, and H-10/H-11) and the HMBC signals from H-2 to C-4/C-5/C-11/C-13, from H-4 to C-5/C-6/C-12, from H-11 to C-7/C-9/C-15, from CH_3-14 to C-4/C-6/C-12, and from H-15 to C-5/C-7/C-11. The trichothecene moiety in compound **1** differs from that in roridin J by the presence of an additional hydroxy group. This hydroxy group at C-3 (δ_C 76.4, δ_H 4.47) was confirmed based on the ^1H–^1H COSY correlations (H-2/H-3/H-4) and HMBCs from H-3 to C-4. The macrocyclic lactone moiety, which is identical to that in roridin J, was confirmed by ^1H–^1H COSY correlations (H-4'/H-5', and H-14'/H-13'/H-6'/H-7'/H-8'/H-9'/H-10') and the HMBC signals from H-2' to C-1'/C-3'/C-4', from CH_3-12' to C-1'/C-2'/C-3'/C-4', from H-4' to C-2'/C-3'/C-5'/C-12', from H-6' to C-7'/C-8'/C-13', from CH_3-14' to C-6'/C-13', and from H-9' to C-7'/C-11'. The connection between the two moieties was established by the presence of two ester bonds, as evidenced by HMBCs from H-4 to C-11′ and from H-15 to C-1′. Therefore, the planar structure of compound **1** was determined.

The relative configuration of the trichothecene moiety in compound **1** was elucidated based on nuclear Overhauser enhancement spectroscopy (NOESY) analysis and the common biosynthetic pathways of trichothecene sesquiterpenes [1, 28, 29]. The NOESY spectrum displayed key correlations, including H-11/H-4, H-11/H-15a, H-2/H-3, H-2/H-13b, CH_3-14/H-13a, and H-3/CH_3-14 (Fig. 3). These correlations suggest that the seven chiral centers in the trichothecene ring of compound **1** are configured as 2*R*,3*R*,4*S*,5*S*,6*R*,11*R*, and 12*S*. In the macrocyclic lactone moiety, the configurations of the double bonds at $\Delta^{2'}$, $\Delta^{7'}$, and $\Delta^{9'}$ were determined to be *E*, *E* and *Z*, respectively, based on the NOESY correlations between H-2′/H-4′, as well as the coupling constants ($^3J_{7',8'}$ = 15.3 Hz, and $^3J_{9',10'}$ = 11.3 Hz). The NOESY correlations of H-5′/H-6′/CH_3-14' and H-4′/H-13′, indicated two possible configurations for the macrocyclic lactone moiety: 4'*R*,5'*R*,6'*S*,13'*S* and 4'*S*,5'*S*, 6'*R*,13'*R*.

To further confirm the relative configuration of compound **1**, GIAO ^{13}C NMR calculations with STS protocol [30] were performed on two isomers, **1a** (2*R*,3*R*,4*S*,5*S*,6*R*,11*R*, 12*S*,4'*R*,5'*R*,6'*S*,13'*S*) and **1b** (2*R*,3*R*,4*S*,5*S*,6*R*,11*R*,12*S*,4'*S*, 5'*S*,6'*R*,13'*R*), at the ωB97x-D/6-31G*//B3LYP-D3(BJ)/TZVP level. The results showed that isomer **1a** had the lowest mean absolute error (MAE) and root mean square (RMS) values compared to the experimental data of compound **1** (Fig.

Table 1 The ^{1}H NMR data (600 MHz) of compounds 1−4 in $CDCl_3$ (*J* in Hz)

No.	1	2	3	4
2	3.65, overlapped	3.82, overlapped	3.84, br d (4.6)	3.86, overlapped
3	4.47, br d (4.2)	2.21, overlapped 2.46, dd (16.2, 8.2)	2.20, m 2.47, dd (15.2, 8.0)	4.37, br s
4	5.56, br s	5.88, m	5.88, m	5.64, br s
7	1.90, m	2.13, m 2.21, overlapped	1.91, m	1.88, m
8	2.02, m	5.19, br s	2.02, m	2.01, m
10	5.52, br s	5.69, br s	5.44, br s	5.53, br s
11	4.01, br s	3.73, br s	3.64, br s	4.05, br s
13	2.78, br s 3.05, br s	2.83, br s 3.10, br s	2.83, br s 3.12, br s	2.78, br s 3.05, br s
14	0.82, s	0.82, s	0.83, s	0.78, s
15	4.06, d (12.6) 4.40, d (12.6)	4.40, q (12.2)	3.90, d (12.6) 4.60, overlapped	3.91, d (12.7) 4.49, overlapped
16	1.73, s	1.75, s	1.71, s	1.72, s
18		1.92, s		
2'	5.75, br s	5.71, br s	6.11, br s	5.75, br s
4'	3.84, br d (5.0)	3.82, overlapped	4.44, br s	2.48, m
5'	5.27, br d (5.0)	5.22, br d (7.1)	4.20, d (12.0) 4.60, overlapped	4.11, m 4.49, overlapped
6'	4.09, m	4.08, d (8.7)		
7'	5.93, br d (15.3)	5.92, d (15.2)	6.02, d (15.7)	6.01, d (15.5)
8'	7.59, t (13.5)	7.62, t (12.0)	8.02, t (13.5)	7.93, dd (15.5, 11.5)
9'	6.56, t (11.3)	6.56, t (11.3)	6.61, t (11.3)	6.63, t, (11.5)
10'	5.83, d (11.3)	5.79, d (11.3)	6.09, d (11.3)	6.16, d (11.5)
12'	2.26, s	2.26, s	2.26, s	2.25, s
13'	3.65, overlapped	3.64, m		
14'	1.37, br s	1.37, d (3.6)		
1"				5.05, s
2"				3.58, overlapped
3"				3.83, overlapped
4"				3.58, overlapped
5"				3.58, overlapped
6"				3.70, overlapped 3.83, overlapped

S39). The absolute configuration of compound **1** was further validated by comparing its experimental and calculated ECD spectra. Calculations for the two possible configurations (**1a** and **1b**) were performed using Gaussian 16 at the ωB97x-D/TZVP//B3LYP-D3(BJ)/TZVP level of theory. The calculated ECD spectrum of **1a** exhibited a positive Cotton effect at 218 nm (Δε +43.8) and a negative Cotton effect at 254 nm (Δε −10.0), closely matching the experimental ECD spectrum of compound**1** (Fig. 4). In contrast, the calculated ECD curve of **1b** showed a positive Cotton effect in the range of

Table 2 The ^{13}C NMR data (150 MHz) of compounds 1–4 in $CDCl_3$

No.	1	2	3	4
2	79.4, CH	79.9, CH	79.2, CH	77.1, CH
3	76.4, CH	34.7, CH_2	34.9, CH_2	81.2, CH
4	82.2, CH	73.5, CH	75.3, CH	81.5, CH
5	49.5, C	49.2, C	49.2, C	49.2, C
6	44.0, C	42.2, C	43.3, C	43.9, C
7	20.6, CH_2	26.4, CH_2	20.6, CH_2	20.5, CH_2
8	27.7, CH_2	68.9, CH	27.8, CH_2	27.6, CH_2
9	140.4, C	136.6, C	140.7, C	140.4, C
10	118.4, CH	124.1, CH	118.8, CH	118.7, CH
11	68.8, CH	67.4, CH	67.7, CH	68.6, CH
12	64.7, C	65.5, C	65.6, C	64.1, C
13	47.3, CH_2	48.0, CH_2	48.1, CH_2	47.1, CH_2
14	7.4, CH_3	7.4, CH_3	7.4, CH_3	7.1, CH_3
15	63.4, CH_2	65.0, CH_2	63.4, CH_2	63.1, CH_2
16	23.5, CH_3	20.7, CH_3	23.4, CH_3	23.3, CH_3
17		171.1, C		
18		21.1, CH_3		
1'	166.0, C	166.4, C	165.9, C	165.7, C
2'	119.7, CH	119.5, CH	115.2, CH	118.1, CH
3'	155.8, C	155.8, C	157.5, C	156.7, C
4'	79.7, CH	79.2, CH	73.6, CH	40.1, CH_2
5'	103.4, CH	103.3, CH	64.9, CH_2	60.4, CH_2
6'	82.5, CH	82.4, CH	166.3, C	166.1, C
7'	135.0, CH	134.6, CH	127.6, CH	128.2, CH
8'	126.0, CH	126.1, CH	140.1, CH	138.5, CH
9'	143.4, CH	143.4, CH	139.2, CH	140.2, CH
10'	118.9, CH	118.5, CH	125.5, CH	124.9, CH
11'	166.3, C	165.6, C	165.7, C	165.5, C
12'	13.4, CH_3	13.1, CH_3	16.1, CH_3	17.2, CH_3
13'	76.6, CH	76.4, CH		
14'	16.1, CH_3	16.0, CH_3		
1"				99.2, CH
2"				71.8, CH
3"				73.5, CH
4"				69.4, CH
5"				72.9, CH
6"				60.9, CH_2

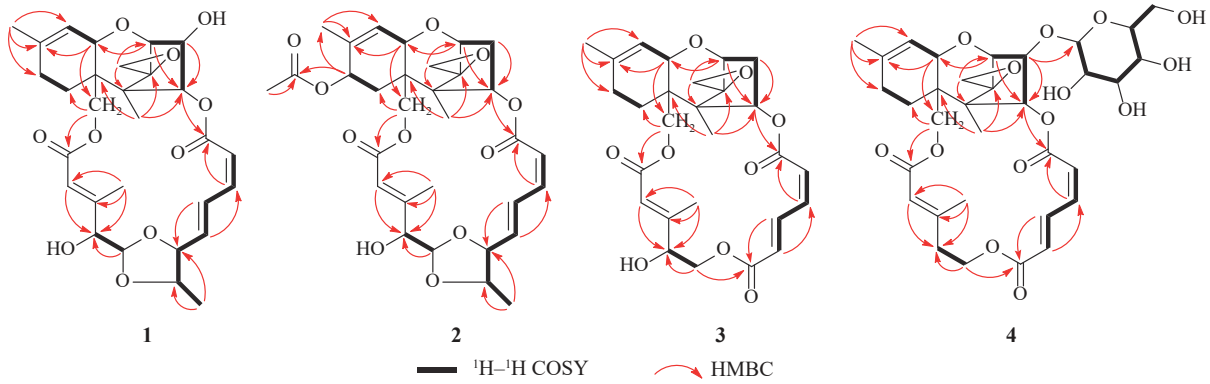

Fig. 2 The key ^{1}H–^{1}H COSY and HMBCs of 1–4.

231–281 nm. Analyzing the excitation of molecular orbitals in structures **1a** and **1b** demonstrated that the configurations in the macrocyclic lactone moiety significantly influenced the excitations to the second lowest unoccupied molecular orbital (LUMO + 1), determining the signs of the Cotton effects in this range (Fig. S42). This analysis further confirmed that the structure of compound **1** is **1a**. Thus, the absolute configuration of compound **1** was determined to be 2*R*,3*R*,4*S*,5*S*,6*R*, 11*R*,12*S*,4'*R*, 5'*R*,6'*S*,13'*S*, and it was named mytoxin D.

Compound **2** was obtained as a white amorphous powder with a molecular formula of $C_{31}H_{38}O_{11}$, as determined by HR-ESI-MS data (*m/z* 604.2762 $[M + NH_4]^+$, Calcd. for $C_{31}H_{42}NO_{11}$, 604.2752). A comparison of the NMR data of **2** with those of roridin J [27] indicated that both compounds share the same core skeleton, with compound **2** differing by the presence of an additional acetyl ester group. This difference was evident from the downfield shifts of C-8 (δ_C 68.9) and H-8 (δ_H 5.19, 1H, br s) and the presence of the acetyl ester group (δ_H 1.92, 3H, s; δ_C 171.1, 21.1). The assignment of the acetyl ester group at C-8 was further confirmed by HMBCs from H-8 to C-6/C-9/C-10/C-17, from CH3-16 and H-7 to C-8, and from CH3-18 to C-17(Fig. 2). A comprehensive analysis of the 2D NMR spectra allowed for the establishment of the planar structure of compound **2**.

The relative configuration of the macrocyclic lactone moiety was determined to be the same as in compound **1**, based on NOESY analysis (Fig. 3). The stereochemistry of the acetyl ester group at C-8 was assigned as *α* based on several lines of evidence. In the ^{13}C NMR spectrum of **2**, the methyl group at C-16 is shifted upfield by 2.6, and C-15 is shifted downfield by 1.8 compared to the chemical shifts of roridin H [31]. When the configuration at C-8 is *β*, the expected upfield shift for C-16 would be around 4–5, while C-15 would show little to no shift [32]. Furthermore, the chemical shifts of compound 2 at C-8, C-15, and C-16 are similar to those of 8*α*-acetoxyroridin H, whose stereochemistry was confirmed through X-ray crystallographic analysis [33]. To further confirm the relative configuration of compound **2**, GIAO ^{13}C NMR calculations with the STS protocol [30] were performed on four isomers: (2*R*,4*R*,5*S*,6*R*,8*R*,11*R*,12*S*,4'*R*,5'*R*, 6'*S*,13'*S*)-**2a**, (2*R*,4*R*,5*S*,6*R*,8*S*,11*R*,12*S*,4'*R*,5'*R*,6'*S*,13'*S*)-**2b**, (2*R*,4*R*,5*S*,6*R*,8*R*,11*R*,12*S*,4'*S*,5'*S*,6'*R*,13'*R*)-**2c**, and (2*R*,4*R*,5*S*, 6*R*,8*S*,11*R*,12*S*,4'*S*,5'*S*,6'*R*,13'*R*)-**2d** at the ωB97x-D/6-31G*//B3LYP-D3(BJ)/TZVP level. The results showed that isomer (8*S*,4'*R*,5'*R*,6'*S*,13'*S*)-**2b** had the lowest MAE and RMS values compared to the experimental data of compound **2**, with a P_{rel} probability of 99.22% (Fig. S40). Subsequently, the ECD spectrum of isomer **2b** was calculated at the ωB97x-D/TZVP//B3LYP-D3(BJ)/TZVP level in methanol with the PCM model. As shown in Fig. 4, the calculated ECD curves of (2*R*,4*R*,5*S*,6*R*,8*S*,11*R*,12*S*,4'*R*,5'*R*,6'*S*,13'*S*)-**2b** matched well with the experimental ECD curves. Therefore, the absolute configuration of compound **2** was assigned as 2*R*,4*R*,5*S*, 6*R*,8*S*,11*R*,12*S*,4'*R*,5'*R*,6'*S*,13'*S*, and it was named mytoxin E.

Compound **3** was isolated as a white amorphous powder with a molecular formula of $C_{27}H_{32}O_9$, as determined by HR-ESI-MS (*m/z* 523.1946 $[M + Na]^+$, Calcd. for $C_{27}H_{33}O_9Na$, 523.1939). The ^{1}H NMR data (Table 1) of **3** indicated the presence of six olefinic protons at δ_H 8.02 (1H, t, *J* = 13.5 Hz, H-8'),6.61(1H,t,*J*=11.3Hz,H-9'),6.11(1H,brs,H-2'),6.09(1H,d, *J* = 11.3 Hz, H-10'), 6.02 (1H, d, *J* = 15.7 Hz, H-7'), and 5.44 (1H, br s, H-10)). Additionally, signals for four oxygenated methines were observed at δ_H 5.88 (1H, m, H-4), 4.44 (1H, brs, H-4'), 3.84 (1H, brd, *J* = 4.6 Hz, H-2), and 3.64 (1H, br s, H-11). Six methylene groups, including three oxygenated ones, appeared at δ_H 4.60 (1H, H-15a), 3.90 (1H, d, *J* = 12.6 Hz, H-15b), 4.60 (1H, H-5'a), 4.20 (1H, d, *J* = 12.0 Hz, H-5'b), 3.12 (1H, brs, H-13a), 2.83 (1H, br s, H-13b), 2.02 (2H, m, H-8), 1.91 (2H, m, H-7), 2.20 (1H, m, H-3a), and 2.47 (1H, dd, *J* = 15.2, 8.0 Hz, H-3b). Three methyl groups were also observed at δ_H 0.83 (3H, s, H-14), 1.71 (3H, s, H-16), and 2.26 (3H, s, H-12'). The ^{13}C NMR spectrum (Table 2) displayed 27 carbon signals, including three ester carbonyls at δ_C 166.3, 165.9, 165.7; eight olefinic carbons at δ_C 157.5, 140.7, 140.1, 139.2, 127.6, 125.5, 118.8, and 115.2, indicative of four double bonds; four oxygenated sp^3 methines at δ_C 79.2, 75.3, 73.6, 67.7, three sp^3 quaternary carbons, including one oxygenated at δ_C 65.6, 49.2, and 43.3; six methylene groups, including three oxygenated ones, at δ_C 64.9, 63.4, 48.1, 34.9, 27.8, and 20.6, and three methyl groups δ_C 23.4, 16.1, and 7.4. The ^{1}H and ^{13}C NMR data of compound **3** were similar to those of verrucarin J [34], with the key difference be-

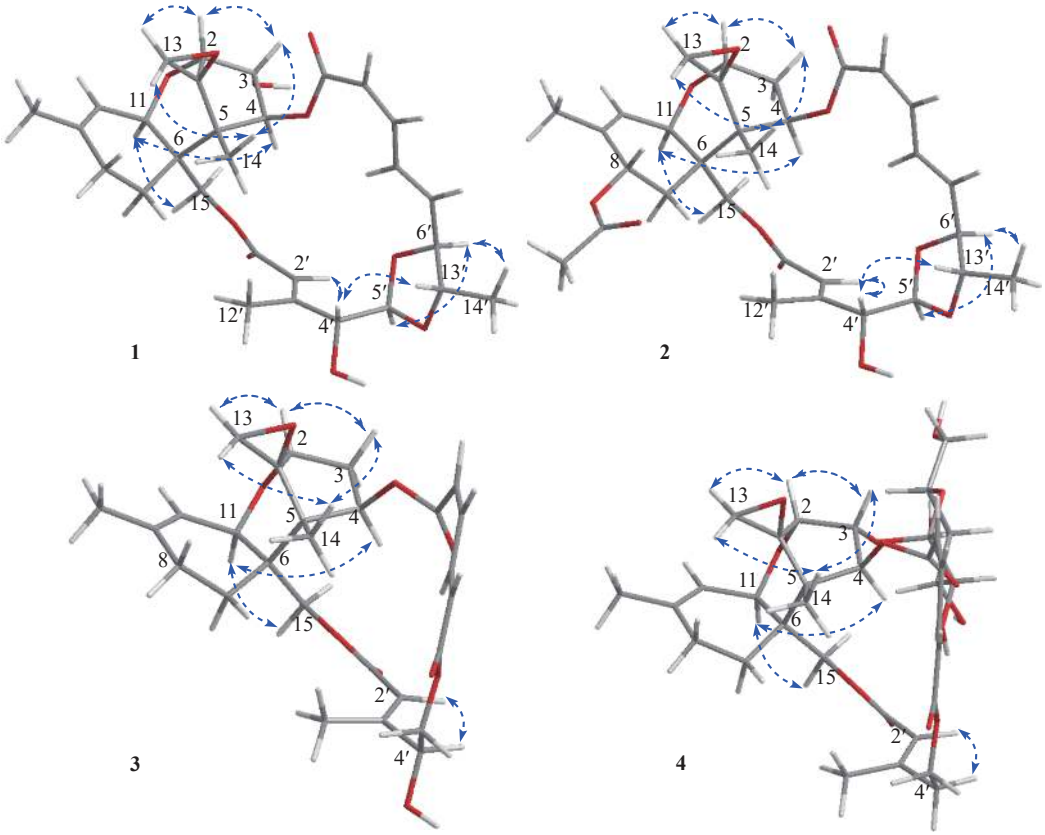

Fig. 3 The key NOESY correlations of 1–4.

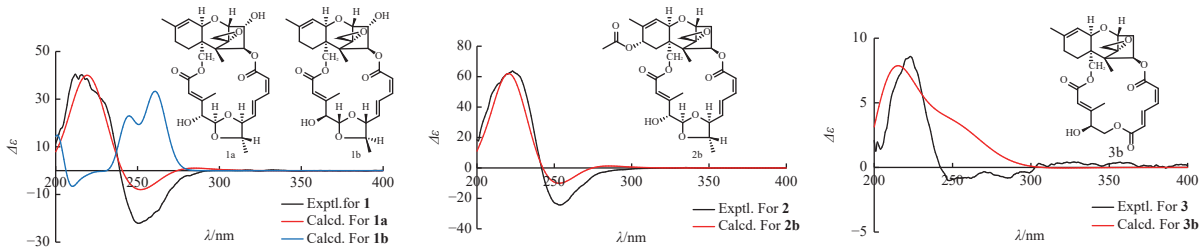

Fig. 4 The experimental and calculated ECD curves of 1–3.

ing an additional hydroxy group at C-4' (δ_H 4.44, δ_C 73.6). This difference was confirmed by ^{1}H–^{1}H COSY correlations (H-4'/H-5') and HMBCs from H-2' to C-4', CH_3-12' to C-4', and H-5' to C4' (Fig. 2). Thus, the planar structure of compound **3** was established.

The relative configuration of the macrocyclic lactone moiety in compound **3** was determined to be the same as that in compound **1**, based on NOESY analysis (Fig. 3). To determine the absolute configuration of C-4', ^{13}C NMR chemical shift calculations were performed for two isomers: (2*R*,4*R*,5*S*,6*R*,11*R*,12*S*,4'*R*)-**3a** and (2*R*,4*R*,5*S*,6*R*,11*R*,12*S*,4'*S*)-**3b**, using the same computational method employed for compound **2**. The results demonstrated that the calculated data for isomer **3b** exhibited lower MAE and RMS values, indicating higher accuracy. Additionally, the P_{mean} and P_{rel} parameters further supported the greater rationality of the **3b** configuration (Fig. S41). The calculated ECD data also reinforced the rationality of the **3b** configuration (Fig. 4). Therefore, the absolute configuration of compound **3** was determined to be 2*R*,4*R*,5*S*,6*R*,11*R*,12*S*,4'*S*, and it was named mytoxin F.

Compound **4** was isolated as a white amorphous powder. The HR-ESI-MS data displayed an $[M + Na]^+$ ion peak at *m/z* 685.2507, indicating a molecular formula of $C_{33}H_{42}O_{14}$ (Calcd. for $C_{33}H_{42}O_{14}Na$, 685.2467). Based on the NMR and HR-ESI-MS data, compound **4** was identified as a derivative of verrucarin J [34] with an additional glucosyl unit. The *α*-configuration of the glucosyl moiety was confirmed by the coupling constant of the anomeric proton (3.4 Hz; Fig. S29) and further supported its D-configuration (Fig. S38), which was determined through hydrolysis, derivatization, and HPLC analysis [35]. The attachment of the *α*-glucopyranosyl moiety at C-3 was indicated by the downfield shifts of C-3 (δ_C 81.2) and H-3 (δ_H 4.37), as well as HMBCs from H-3 to C-1" (Fig. 2). Additionally, the *α*-configuration at C-3 was confirmed by

NOESY correlations between H-3 and CH_3-14 (Fig. 3). Consequently, the structure of compound **4** was established and named mytoxin G.

Four known compounds were identified as 8*α*-acetoxyroridin H (**5**) [32], roridin J (**6**) [27], verrucarin J (**7**) [34], and verrucarin L (**8**) [36] by comparing their spectral data with those reported in the literature.

Given that trichothecene analogs have potent cytotoxic properties [17, 18], all isolated compounds were evaluated for their *in vitro* cytotoxicity against human oral squamous cell carcinoma CAL27 cell lines and human colorectal cancer HCT116 cell lines using the CCK-8 assay, with 5-fluorouracil as the positive control. As shown in Table 3, exhibited significant inhibitory effects against both CAL27 and HCT116 cell lines, with IC_{50} values ranging from 3 to 6 nmol·L^{-1}, surpassing the efficacy of 5-fluorouracil. The effects of compounds **1** and **3** on HCT116 cell apoptosis were evaluated using an annexin V-FITC and propidium iodide (PI) double staining flow cytometric assay. This analysis revealed a marked increase in the rate of cell apoptosis (Fig. 5). Caspase 3, the primary effector caspase in apoptosis [37], was assessed *via* a caspase-3 activity assay kit, which showed a noticeable increase in caspase-3 activation after treatment with compounds **1** and **3** (Fig. 5). Structure-activity relationship (SAR) analysis revealed that cytotoxicity was significantly reduced by the presence of an acetyl ester group at position C-8, as demonstrated by the contrasting activity levels of compounds **1** and **6** compared to compounds **2** and **5**. Additionally, the comparison of activity levels between compounds **3**, **4**, **7**, and **8** indicated that the inclusion of a glucosyl moiety at position C-3 also led to a decrease in cytotoxicity.

Conclusion

Soil fungi have been instrumental in the discovery of structurally unique and biologically potent secondary metabolites. Recently, there has been growing interest in their potential to produce pharmaceutically significant lead compounds. This study comprehensively isolated eight macrocyclic trichothecenes from the soil fungus *Myrothecium verrucaria*, including four previously unreported compounds. These compounds are characterized by an EPT core and can be categorized as roridins with a C_{29} skeleton or verrucarins with a C_{27} skeleton. Notably, compound **4** is the first macrocyclic trichothecene to feature a glucosyl unit within the trichothecene moiety. The structures of these compounds were elucidated through extensive spectroscopic analysis, supported by biosynthetic pathway insights and quantum chemical calculations, including ^{13}C NMR and ECD calculations. The cytotoxicity assays yielded promising results, highlighting the significant cytotoxic effects exhibited by the majority of these compounds. Furthermore, SAR analysis revealed that the presence of an acetyl ester group at C-8 or a glucosyl moiety at C-3 significantly reduces cytotoxicity. This study not only expands the structural diversity of macrocyclic trichothecenes but also underscores their potential as potent chemotherapeutic agents for cancer treatment. Future research should focus on elucidating the precise mechanisms of action and optimizing the efficacy and toxicity profiles of these macrocyclic trichothecenes, paving the way for their potential application in clinical settings.

Table 3 The cytotoxic activities of compounds 1–8 (IC_{50}, nmol·L^{-1}, mean ± SD, n = 3)

Compound	Cal27 cell lines	HCT116 cell lines
1	5.63 ± 0.46	3.12 ± 1.59
2	107.35 ± 11.78	44.43 ± 7.39
3	3.53 ± 0.10	5.80 ± 0.20
4	1584.33 ± 102.77	1782.33 ± 67.05
5	174.30 ± 5.53	87.28 ± 3.21
6	8.50 ± 0.27	8.50 ± 0.88
7	10.07 ± 0.83	12.71 ± 0.71
8	13.13 ± 1.26	9.72 ± 0.38
5-Fluorouracil	5723.00 ± 648.88	2844.67 ± 208.21

Experimental

General experimental procedures

UV spectra were recorded using a Cary 300 spectrometer (Agilent Technologies, Santa Clara, CA, USA). Circular Dichroism (CD) spectra were obtained on a Chirascan™-plus Circular Dichroism spectrometer. Optical rotations were measured with a Rudolph Research Analytical Autopol IV automatic polarimeter. IR spectra were recorded on a Shimadzu Fourier Transform Infrared Spectrometer using KBr pellets. High-resolution electrospray ionization mass spectrometry (HR-ESI-MS) spectra were acquired with an Agilent 6500 series Q-TOF mass spectrometer (Agilent Technologies, Singapore). NMR spectra were recorded at 600 MHz for ^1H and 150 MHz for ^{13}C on Bruker spectrometers (Bruker BioSpin, Rheinstetten, Germany). Column chromatography (CC) was performed using macroporous adsorbent resin D101 (Tianjin Haoju Resin Technology Co., Ltd., Tianjin, China), silica gel (200−300 mesh, Qingdao Marine Chemical, Qingdao, China), and Sephadex LH-20 (GE Healthcare, Uppsala, Sweden). HPLC separations were conducted using an Agilent 1260 system, which included an automatic sampler, a pump, and a wavelength absorbance detector, along with an Agilent semipreparative column (9.4 mm × 150 mm, C_{18}, 5 μm) (Agilent Technologies). Additionally, an EClassical P3500 prep-HPLC system equipped with a Supersil ODS-2 column (Elite, 5 μm, 10 mm × 250 mm) and a DAD detector (EClassical P3500, Dalian Elite Analytical Instruments Co., Ltd., Dalian, China) was used. Thin-layer chromatography (TLC) separations were performed on precoated silica gel GF_{254} plates (Qingdao Marine Chemical), with spots visualized under UV light (254 or 356 nm) or by spraying with 10% H_2SO_4 in ethanol followed by heating.

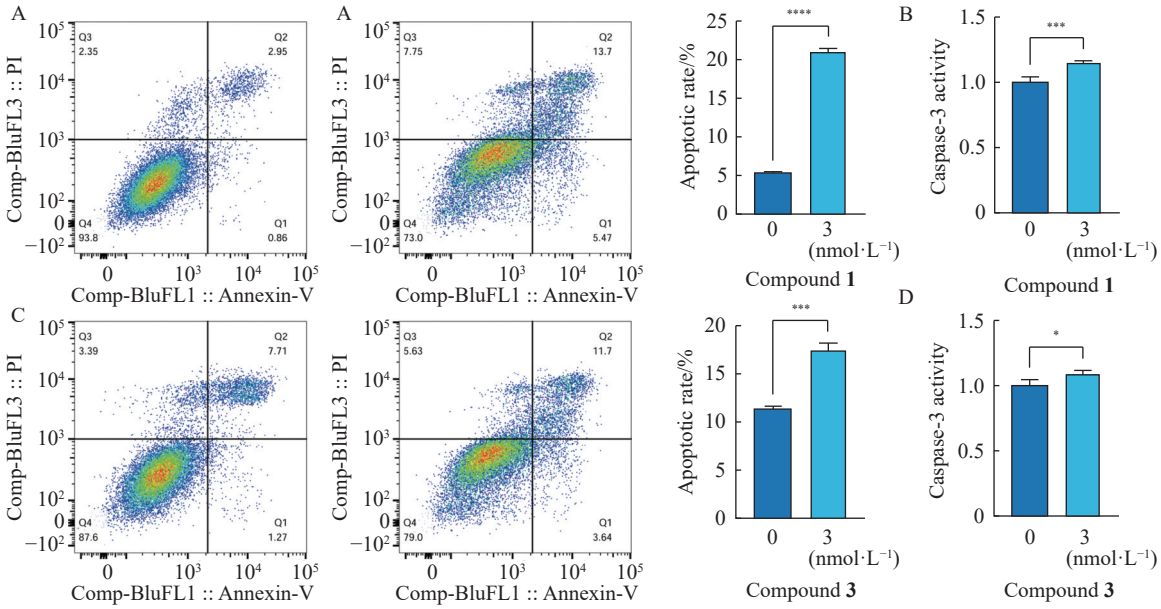

Fig. 5 Compounds 1 and 3 induce cell apoptosis and activate the caspase-3 in HCT116 cells. (A) Flow cytometry to determine apoptosis rates of HCT116 cells after treatment with concentration at 3 nmol·L^{-1} of compound 1 for 24 h, followed by staining with annexin V-FITC/PI. The column shows apoptosis rates of HCT116 cells. Apoptosis rates were calculated by the sum of early and late apoptotic cells. (B) Caspase-3 activity assay on HCT116 cells after treatment with compound 1 for 24 h. (C) Flow cytometry to determine apoptosis rates of HCT116 cells after treatment with concentration at 2 nmol·L^{-1} of compound 3 for 24 h, followed by staining with annexin V-FITC/PI. The column shows apoptosis rates of HCT116 cells. Apoptosis rates were calculated by the sum of early and late apoptotic cells. (D) Caspase-3 activity assay on HCT116 cells after treatment with compound 3 for 24 h. The data are expressed as mean ± SD (n = 3). $^{*}P$ < 0.05, $^{**}P$ < 0.001, $^{****}P$ < 0.0001 *vs* control group.

Fungal material

The fungal strain PA57 was isolated from a soil sample collected from Daweishan Forest Park, Hunan Province, China, in 2020. This strain was identified as *Myrothecium verrucaria* based on ITS sequencing, with a percentage identity of 99.09% to *M. verrucaria* KR708633.1 for ITS4 (Table S15). The fungal specimen is deposited at the Xiangya School of Pharmaceutical Sciences, Central South University, Changsha, China.

Fermentation and isolation

The fungal strain was initially cultivated on potato dextrose agar for 8 days at 25 °C. The mycelia were then cut into pieces and cultured on a cooked rice medium, prepared by mixing 100 g of rice with 80 mL of water in 500 mL Erlenmeyer flasks. The total weight of the rice used was 5 kg. The rice cultures were maintained at 25 °C for 30 d. After the incubation period, the rice was cut into small pieces and extracted with 20 L of ethyl acetate at room temperature over five extraction cycles. The solvent was then evaporated under vacuum to yield 105 g of crude extract. The crude extract was adsorbed onto D101 macroporous resin and eluted stepwise with water, 80% methanol, and 100% methanol. The 80% methanol fraction was subjected to silica gel CC and eluted with a gradient of petroleum ether/ethyl acetate (1 ∶ 0 to 1 ∶ 1) to yield 25 fractions (Fr. 1−Fr. 25). Fraction 11 was purified by preparative HPLC using a methanol/water gradient (30 ∶ 70 to 70 ∶ 30, 30 min, 2.0 mL·min^{-1}, C_{18} column) to yield compound 4 (10.0 mg, t_R 30.0 min). Fraction 18 was separated by Sephadex LH-20 chromatography (methanol) to afford five subfractions (Fr. 18.1−Fr. 18.5). Subfraction Fr. 18.2 was further purified by preparative HPLC using an acetonitrile/water gradient (40 ∶ 60 to 87 ∶ 13, 30 min, 3.0 mL·min^{-1}, Supersil ODS-2 column) to yield compound **5** (5.3 mg, t_R 24.5 min) and compound **7** (3.7 mg, t_R 23.0 min). Fraction 20 was purified by preparative HPLC using a methanol/water mixture (68 ∶ 32, 35 min, 3.0 mL·min^{-1}, Supersil ODS-2 column) to yield compound **6** (3.0 mg, t_R 16.4 min). Fraction 21 was separated by Sephadex LH-20 chromatography (methanol) to afford six subfractions (Fr. 21.1−Fr. 21.6). Subfraction Fr. 21.3 was further purified by preparative HPLC using a methanol/water gradient (48 ∶ 52 to 68 ∶ 32, 35 min, 2.0 mL·min^{-1}, C_{18} column) to obtain compound **1** (3.2 mg, t_R 17.6 min), compound **2** (2.5 mg, t_R 27.2 min), compound **3** (2.0 mg, t_R 22.1 min), and compound **8** (4.5 mg, t_R 19.9 min).

*Mytoxin D (**1**)*: white amorphous powder; $[\alpha]_D^{25}$ 22.1 (*c* 0.71, MeOH); UV (MeOH−H_2O) λ_{max} (log ε) 225 (2.50), 260 (1.80) nm; IR (KBr) ν_{max} 3678, 1717, 1519, 1286, 1168, 818cm^{-1}; ^{1}H NMR (600 MHz, $CDCl_3$) and ^{13}C NMR (150 MHz, $CDCl_3$) (Tables 1 and 2); HR-ESI-MS (positive) *m/z* 562.2687 $[M + NH_4]^+$ (Calcd. for $C_{29}H_{40}NO_{10}$, 562.2647).

*Mytoxin E (**2**)*: white amorphous powder; $[\alpha]_D^{25}$ 28.5 (*c* 0.20, MeOH); UV (MeOH−H_2O) λ_{max} (log ε) 225 (4.50), 260 (4.57) nm; IR (KBr) ν_{max} 3679, 3572, 3416, 1711, 1639, 1437, 1240, 1187, 1079, 1032, 971, 820, 613cm^{-1}; ^{1}H NMR (600 MHz, $CDCl_3$) and ^{13}C NMR (150 MHz, $CDCl_3$), see

Tables 1 and 2) HR-ESI-MS (positive) *m/z* 604.2762 [M + NH_4]$^+$ (Calcd. for $C_{31}H_{42}NO_{11}$, 604.2752).

*Mytoxin F (**3**)*: white amorphous powder; $[\alpha]_D^{25}$ 7.9 (*c* 0.44, MeOH); UV (MeOH−H_2O) λ_{max} (log ε) 225 (1.15), 265 (1.10) nm; IR (KBr) ν_{max} 3715, 3423, 2920, 2852, 1716, 1656, 1436, 1275, 1216, 1182, 1150, 1082, 1037, 1000, 968, 880, 820, 646cm^{-1}; ^{1}H NMR (600 MHz, $CDCl_3$) and ^{13}C NMR (150 MHz, $CDCl_3$) (Tables 1 and 2); HR-ESI-MS (positive) *m/z* 523.1946 [M + Na]$^+$ (Calcd. for $C_{27}H_{33}O_9Na$, 523.1939).

*Mytoxin G (**4**)*: white amorphous powder; $[\alpha]_D^{25}$ 52.9 (*c* 2.48, MeOH); UV (MeOH−H_2O) λ_{max} (log ε) 230 (3.25), 265 (3.20) nm; IR (KBr) ν_{max} 3692, 3406, 2922, 1717, 1444, 1356, 1277, 1227, 1171, 1076, 1044, 966, 883, 824, 700, 625 cm^{-1}; ^{1}H NMR (600 MHz, $CDCl_3$) and ^{13}C NMR (150 MHz, $CDCl_3$) (Tables 1 and 2) HR-ESI-MS (positive) *m/z* 685.2507 [M + Na]$^+$ (Calcd. for $C_{33}H_{42}O_{14}Na$, 685.2467).

Quantum chemical calculations

GIAO ^{13}C NMR and ECD calculations for compounds **1**−**3** were performed as previously described [25].

Absolute configuration determination of sugar moiety

The absolute configuration of the sugar moiety in compound **4** was determined using a modified version of a previously described method [36]. Compound **4** (2 mg) was hydrolyzed with 5 mL of 2 mol·L^{-1} HCl for 6 h at 85 °C. The resulting mixture was evaporated to dryness under vacuum, and the residue was dissolved in water and extracted with chloroform. The aqueous layer was then dried under vacuum, and the residue was dissolved in 5 mL of pyridine containing 4 mg of L-cysteine methyl ester and heated at 60 °C for 1 h. Subsequently, 20 μL of o-tolyl isothiocyanate was added, and the mixture was heated at 60 °C for an additional hour. The reaction mixture was directly analyzed using an EClassical P3100 analytical HPLC with a Supersil ODS-2 column (Elite, 5 μm, 4.6 mm × 250 mm) at 25 °C, employing isocratic elution with a mixture of acetonitrile and water (25 ∶ 75, *V/V*) for 30 min at a flow rate of 1.0 mL·min^{-1}. Detection was performed using a UV detector at 250 nm. The retention times (t_R) of the D- and L-glucose derivatives, prepared similarly, were 19.7 and 17.9 min, respectively. D-glucose was identified in compound **4** based on the peak at 19.7 min.

Cytotoxicity assay against CAL27 and HCT116 cell lines

All isolated compounds were evaluated for their cytotoxicity against human oral squamous cell carcinoma CAL27 cell lines and human colorectal cancer HCT116 cell lines using the CCK-8 assay, with 5-fluorouracil as the positive control. Cells were cultured in DMEM medium supplemented with 10% fetal bovine serum and 1% penicillin-streptomycin and incubated in a humidified atmosphere at 37 °C with 5% CO_2. Cell lines were seeded into 96-well plates at a density of 10 000 cells per well and incubated for 24 h at 37 °C with 5% CO_2. After incubation, the cells were treated with the test compounds prepared in culture media at six different concentrations for 48 h. Blank controls (wells with CCK-8, without cells) and negative controls (wells with solution, without samples) were included. Finally, 10 μL of CCK-8 was added to each well and incubated for 1−4 h, after which absorbance was measured at 450 nm using a microplate reader (Feyond-A300, Allsheng, Hangzhou, China). The IC_{50} values were calculated using GraphPad Prism 9.5.1 software.

Apoptosis and Caspase-3 activity determination

The apoptosis of HCT116 cells was assessed using the Annexin V-FITC/PI double-staining method with a kit obtained from Vazyme Biotech Co., Ltd. (Nanjing, China). HCT116 cells were treated with compounds 1 (3 nmol·L^{-1}) and 3 (2 nmol·L^{-1}) for 24 h, harvested, and washed twice with PBS. The cells were then resuspended in 100 μL of 1× binding buffer, followed by the addition of 5 μL each of Annexin V-FITC and PI staining solution. After a 10-min incubation, 400 μL of 1× binding buffer was added, and the cells were analyzed by flow cytometry to determine the ratio of apoptotic cells. Caspase-3 activity was measured using a caspase-3 activity assay kit (Beyotime Institute of Biotechnology, Shanghai, China) according to the manufacturer's instructions. Following treatment with the compounds, cells were incubated in a fresh culture medium containing 5 μmol·L^{-1} substrate for 30 min at room temperature in the dark. The samples were then analyzed at 405 nm using a plate reader.

Supplementary Information

The 1D (^{1}H, ^{13}C, and DEPT 90°, 135° NMR), 2D NMR (^{1}H−^{1}H COSY, HSQC, HMBC, and NOESY), UV, IR, and HR-ESI-MS spectra, as well as quantum chemical calculation data and ITS sequence data, are available in the Supplementary Information. These can be requested by emailing the corresponding authors.

References

[1] Proctor RH, McCormick SP, Gutierrez S. Genetic bases for variation in structure and biological activity of trichothecene toxins produced by diverse fungi [J]. *Appl Microbiol Biotechnol*, 2020, **104**(12): 5185-5199.

[2] Wang J, Zhang M, Yang J, *et al*. Type A trichothecene metabolic profile differentiation, mechanisms, biosynthetic pathways, and evolution in *Fusarium* species: a mini review [J]. *Toxins*, 2023, **15**(7): 446.

[3] Safwan S, Wang SW, Hsiao G, *et al*. New trichothecenes isolated from the marine algicolous fungus *Trichoderma brevicompactum* [J]. *Mar Drugs*, 2022, **20**(2): 80.

[4] Iida A, Konishi K, Kubo H, *et al*. Trichothecinols A, B and C, potent anti-tumor promoting sesquiterpenoids from the fungus *Trichothecium roseum* [J]. *Tetrahedron Lett*, 1996, **37**(51): 9219-9220.

[5] Liu HX, Liu WZ, Chen YC, *et al*. Cytotoxic trichothecene macrolides from the endophyte fungus *Myrothecium roridum* [J]. *J Asian Nat Prod Res*, 2016, **18**(7): 684-689.

[6] Zhao L, Liu L, Wang N, *et al*. Potent toxic macrocyclic trichothecenes from the marine-derived fungus *Myrothecium verrucaria* Hmp-F73 [J]. *Nat Prod Commun*, 2011, **6**(12): 1915-1916.

[7] Zhu MZ, Cen YF, Ye W, *et al*. Recent advances on macrocyclic trichothecenes, their bioactivities and biosynthetic pathway [J]. *Toxins*, 2020, **12**(6): 417.

[8] Grove J. Macrocyclic trichothecenes [J]. *Nat Prod Rep*, 1993, **10**(5): 429-448.
[9] Mondol MA, Surovy MZ, Islam MT, *et al*. Macrocyclic trichothecenes from *Myrothecium roridum* strain M10 with motility inhibitory and zoosporicidal activities against *Phytophthora nicotianae* [J]. *J Agric Food Chem*, 2015, **63**(40): 8777-8786.
[10] Zhang SY, Li ZL, Guan LP, *et al*. Structure determination of two new trichothecenes from a halotolerant fungus *Myrothecium* sp GS-17 by NMR spectroscopy [J]. *Magn Reson Chem*, 2012, **50**(9): 632-636.
[11] Li TX, Xiong YM, Chen X, *et al*. Antifungal macrocyclic trichothecenes from the insect-associated fungus *Myrothecium roridum* [J]. *J Agric Food Chem*, 2019, **67**(47): 13033-13039.
[12] Liu JY, Huang LL, Ye YH, *et al*. Antifungal and new metabolites of *Myrothecium* sp. Z16, a fungus associated with white croaker *Argyrosomus argentatus* [J]. *J Appl Microbiol*, 2006, **100**(1): 195-202.
[13] Lakornwong W, Kanokmedhakul K, Soytong K, *et al*. Types A and D trichothecene mycotoxins from the fungus *Myrothecium roridum* [J]. *Planta Med*, 2019, **85**(09/10): 774-780.
[14] Zhang HJ, Tamez PA, Aydogmus Z, *et al*. Antimalarial agents from plants. III. trichothecenes from *Ficus fistulosa* and *Rhaphidophora decursiva* [J]. *Planta Med*, 2002, **68**(12): 1088-1091.
[15] Isaka M, Punya J, Lertwerawat Y, *et al*. Antimalarial activity of macrocyclic trichothecenes isolated from the fungus *Myrothecium verrucaria* [J]. *J Nat Prod*, 1999, **62**(2): 329-331.
[16] Waterman C, Calcul L, Mutka T, *et al*. A potent antimalarial trichothecene from *hyphomycete* species [J]. *Tetrahedron Lett*, 2014, **55**(29): 3989-3991.
[17] Lee SR, Seok S, Ryoo R, *et al*. Macrocyclic trichothecene mycotoxins from a deadly poisonous mushroom, *Podostroma cornu-damae* [J]. *J Nat Prod*, 2019, **82**(1): 122-128.
[18] Shen L, Ai CZ, Song YC, *et al*. Cytotoxic trichothecene macrolides produced by the endophytic *Myrothecium roridum* [J]. *J Nat Prod*, 2019, **82**(6): 1503-1509.
[19] Amagata T, Rath C, Rigot JF, *et al*. Structures and cytotoxic properties of trichoverroids and their macrolide analogues produced by saltwater culture of *Myrothecium verrucari*a [J]. *J Med Chem*, 2003, **46**(20): 4342-4350.
[20] Chandrasekaran B, Tyagi A, Sharma AK, *et al*. Molecular insights: suppression of EGFR and AKT activation by a small molecule in non-small cell lung cancer [J]. *Genes cancer*, 2017, **8**(9-10): 713-724.
[21] Deeb D, Gao XH, Liu YB, *et al*. The inhibition of cell proliferation and induction of apoptosis in pancreatic ductal adenocarcinoma cells by verrucarin A, a macrocyclic trichothecene, is associated with the inhibition of Akt/NF-B/mTOR prosurvival signaling [J]. *Int J Oncol*, 2016, **49**(3): 1139-1147.
[22] Pal D, Tyagi A, Chandrasekaran B, *et al*. Suppression of Notch1 and AKT mediated epithelial to mesenchymal transition by verrucarin J in metastatic colon cancer [J]. *Cell Death Dis*, 2018, **9**(8): 798.
[23] Palanivel K, Kanimozhi V, Kadalmani B, *et al*. Verrucarin A induces apoptosis through ROS-mediated EGFR/MAPK/Akt signaling pathways in MDA-MB-231 breast cancer cells [J]. *J Cell Biochem*, 2014, **115**(11): 2022-2032.
[24] Yan F, Yu Y, Chow DC, *et al*. Identification of verrucarin A as a potent and selective steroid receptor coactivator-3 small molecule inhibitor [J]. *PLoS One*, 2014, **9**(4): e95243.
[25] Wu XQ, Li J, Zhou X, *et al*. Liver-cell protective pyridones from the fungi *Tolypocladium album* dws120 [J]. *Phytochemistry*, 2023, **212**: 113730.
[26] Wang J, Wu XQ, Mo JS, *et al*. Two pairs of new isobenzofuranone enantiomers from a soil-derived fungus *Penicillium canescens* DWS225 [J]. *Nat Prod Res*, 2023, **11**: 1-9.
[27] Matsumoto M, Ito A, Tonouchi A, *et al*. Stereochemical correction and total structure of roridin J [J]. *Tetrahedron*, 2017, **73**(36): 5430-5435.
[28] Desjardins AE. From yellow rain to green wheat: 25 years of trichothecene biosynthesis research [J]. *J Agric Food Chem*, 2009, **57**(11): 4478-4484.
[29] Alexander NJ, Proctor RH, McCormick SP. Genes, gene clusters, and biosynthesis of trichothecenes and fumonisins in *Fusarium* [J]. *Toxin Rev*, 2009, **28**(2-3): 198-215.
[30] Li J, Liu JK, Wang WX. GIAO C-13 NMR calculation with sorted training sets improves accuracy and reliability for structural assignation [J]. *J Org Chem*, 2020, **85**(17): 11350-11358.
[31] Yu NJ, Guo SX, Lu HY. Cytotoxic macrocyclic trichothecenes from the mycelia of *Calcarisporium arbuscula Preuss* [J]. *J Asian Nat Prod Res*, 2002, **4**(3): 179-183.
[32] Breitenstein W, Tamm C. ^{13}C-NMR-spectroscopy of the trichothecane derivatives verrucarol, verrucarins A and B and roridins A, D and H [J]. *Helv Chim Acta*, 1975, **58**(4): 1172-1180.
[33] Wagenaar MM, Clardy J. Two new roridins isolated from *Myrothecium* sp. [J]. *J Antibiot*, 2001, **54**(6): 517-520.
[34] Jarvis BB, Stahly GP, Pavanasasivam G, *et al*. Isolation and characterization of the trichoverroids and new roridins and verrucarins [J]. *J Org Chem*, 1982, **13**: 1117-1124.
[35] Tanaka T, Nakashima T, Ueda T, *et al*. Facile discrimination of aldose enantiomers by reversed-phase HPLC [J]. *Chem Pharm Bull*, 2007, **55**(6): 899-901.
[36] Jarvis BB, Midiwo JO, DeSilva T, *et al*. Verrucarin L, a new macrocyclic trichothecene [J]. *J Antibiot*, 1981, **34**(1): 120-121.
[37] Carneiro BA, El-Deiry WS. Targeting apoptosis in cancer therapy [J]. *Nat Rev Clin Oncol*, 2020, **17**(7): 395-417.

Cite this article as: MO Jisong, TAN Yufen, AI Wenjing, *et al*. Macrocyclic trichothecenes from *Myrothecium verrucaria* PA 57 and their cytotoxic activity [J]. *Chin J Nat Med*, 2024, **22**(9): 854-863.